Direct Measurements of Reynolds Stresses and Turbulence in the Bottom Boundary Layer

Joseph Katz
Department of Mechanical Engineering, and
Center for Environmental and Applied Fluid Mechanics
Johns Hopkins University, 3400 N. Charles Street
Baltimore, MD 21218
phone: (410) 516-5470 fax: (410) 516-7254 email: katz@titan.me.jhu.edu

Thomas Osborn
Department of Earth and Planetary Sciences, and
Center for Environmental and Applied Fluid Mechanics
The Johns Hopkins University
3400 N Charles Street
Baltimore, MD 21218-2681
phone (410) 516-7039 fax (410) 516-7933 email osborn@jhu.edu
Award Number: N000149510215

LONG-TERM GOALS

a) Measure the Reynolds stresses, velocity profile, vorticity, dissipation, and turbulent spectra in the bottom boundary layer of the coastal ocean using particle imaging velocimetry (PIV). The validity of these direct stress measurements is independent of assumptions about the boundary layer structure, turbulent spectra and balance of production and dissipation.
b) Quantify the temporal variation of turbulent stresses in relation to the oceanographic parameters that represent the local environment, such as waves, currents, vertical density gradient, internal waves and nature of the water-sediment interface. The conclusions will be used to determine the relative importance of different mechanisms, which control the flow and turbulence in the benthic boundary layer of the coastal ocean.
c) Quantify the spatial variation of the stress in different environments to determine the relationship between point measurements and spatial averages, that are necessary for numerical modeling of coastal currents.

OBJECTIVES

The objective of this project is to directly measure the flow structure and turbulence, including the Reynolds stress, in the bottom boundary layer of the coastal ocean using particle image velocimetry (PIV).

APPROACH

Particle image velocimetry (PIV) is capable of mapping two components of the instantaneous velocity distribution within an entire section of a flow field. This method consists of illuminating the fluid with a laser sheet while seeding the water with microscopic tracer particles. In oceanic applications the natural seeding, as available data and our own experience indicate, is sufficient. If the laser is pulsed more than once while recording a single (or two) image(s), each particle leaves multiple traces on the same (or successive) recording medium (media). The most popular approach to data analysis consists

of dividing the image into a large number of small windows and computing the mean displacement of all the particles within each window. Typically, the analysis is based on computing the auto-correlation function of the intensity distribution within the selected window.

Unlike point sensors, a sequence of PIV measurements provides a time series of the spatial distribution, not just a time series of velocity at a single point. Such data enables measurements of the vorticity distribution, rates of strain, turbulent stresses, turbulent spectra, spatial and temporal correlations, energy dissipation. In previous reports and also in a series of recent papers (Bertuccioli et al., 1999; Doron et al., 1999a, b) we describe a submersible PIV system that has been developed for measuring the velocity distribution in the bottom boundary layer of the coastal ocean. This system records up to 15 image pairs/s, although we have mostly recorded data at 1 Hz. The camera that has been deployed until today has a resolution of 1K x 1K pixels2 and each instantaneous vector array consists of 29x29 vectors. Further details are described in the references mentioned above and reports provided in previous years.

WORK COMPLETED

Most of the effort during the past year has focused on analysis of data obtained in a series of tests performed in New York Bight, 7 miles east of Highlands, NJ. In the previous report we described a series of "short time" (132 s) measurements performed at different elevations above the bottom, starting from 10 cm, up to 1.40 much. With data recorded at 1 Hz, we obtained 130 vector maps of 10 cm wide "flow strips" at each of the six elevation. As described in the next section, during FY 99 we have performed considerable data analysis using these results, including computations of turbulent spectra and evaluation of various methods to determine the dissipation rate. In addition, we also recorded longer data sets at 2 Hz for 24 minutes. The resulting more than 2800 vector maps at each elevation provided sufficient data for convergence, longer range of wavenumbers and most important, sufficient data for reliable statistics. Sample results are provided in the next section.

RESULTS

Individual velocity distributions can be used for obtaining true spatial spectra for the range of wavenumbers covered with an individual image. We also combined a series of successive vector maps into an extended "panoramic" view on the flow structure, using the Taylor Hypothesis and displacing individual realizations by the instantaneous mean velocity multiplied by the delay between them (1 s for the short series). This extended data base enabled us to extend to length (time) scales that exceed the range covered by individual maps. Further details on the matching process can be found in Bertuccioli at al. (1999) and Doron et al. (1999). Comparisons between the extended series and averaged true spatial spectra are presented in Figure 1. The short series are all within the inertial and dissipation range whereas the long series extend to The slight differences are attributed to the effect of interpolations in the extended series that "smear" some of the high wavenumber energy as well as the effect of surface waves.

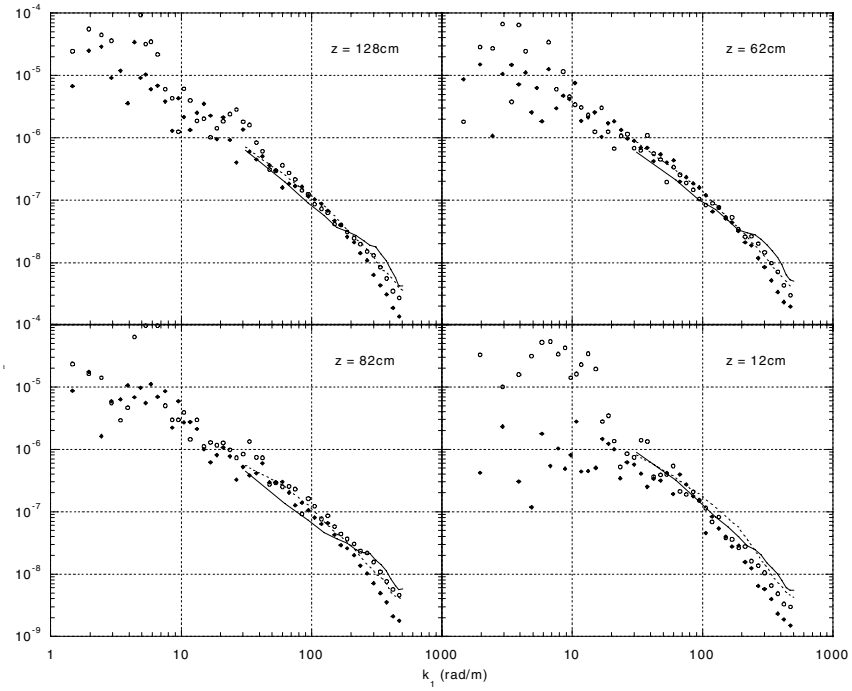

Figure 1: A comparison between true spatial spectra obtained from individual vector maps (solid lines) and extended spectra determined by patching 130 vector maps using the Taylor Hypothesis.

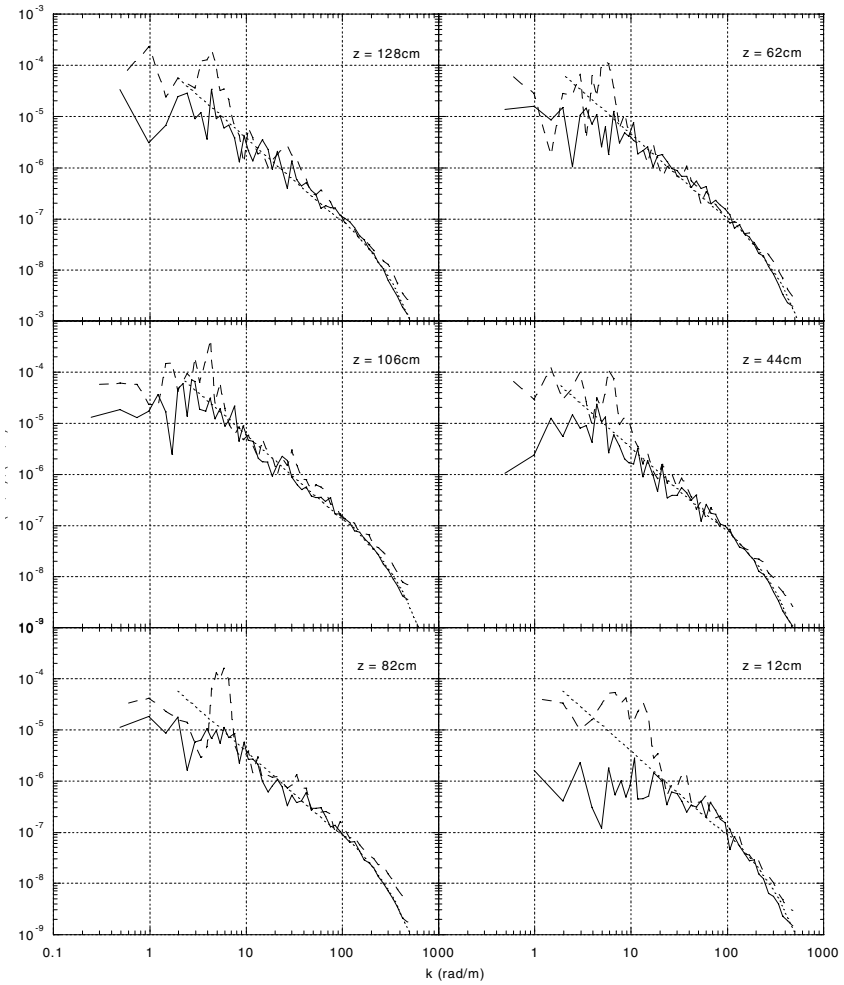

Figure 2: Sample spectra calculated from the extended vector map. Solid lines – E_{11}; Dashed lines – E_{33}; Dotted lines – Nasmyth universal spectrum (which has a (-5/3) slope in the inertial range). The spikes in the horizontal spectra are a result of wave-induced motion (verified by comparison to pressure transducer measurements).

Samples of extended spectra for the short data series are presented in Figure 2. In order to enable a clear view of the trends, the data shown is band-averaged onto a grid of 20 bins per decade. The Nasmyth universal spectrum, based on the numerical values given by Oakey (1982) is also presented. The range of resolved wavenumbers spans about 3 orders of magnitude, except near the floor, where it is slightly smaller. For scales up to the size of a vector map ($k_1 > 31$ rad/m), the spectra are derived from spatial distributions that are directly measured, though they are slightly modified by the interpolation as discussed above. The spectra contain only small regions with horizontal tails (that are characteristic of high frequency white noise), at $k_1 > 400$ rad/m, corresponding to wavelengths of less than 1.6 cm.

At $k_1 <$ 8-10, $E_{11} > E_{33}$ at all elevations. The substantially larger energy content of the horizontal velocity fluctuations is due to the anisotropy of the turbulence and to the effect of the wave induced motion, especially in the region of high peaks. Note that the anisotropy at very low wavenumbers, where both E_{11} and E_{33} seem to reach some plateau, extends beyond the domain affected by surface waves. The jaggedness of the spectra in this range is caused by the small number of data points used for evaluating E_{ii}. The difference between E_{11} and E_{33} is most significant near the sea floor, and decreases with increasing distance from the bottom. Although E_{11} changes shape at low wavenumbers, the characteristic peak magnitudes remain at the same level. On the other hand, the characteristic peak magnitude of E_{33} decreases by more than an order of magnitude between z = 128 cm and z = 12 cm. This trend has been observed in laboratory measurements of flow in turbulent boundary layers, and has led to setting the distance from the wall as the integral length scale, l, for boundary layer flow. Consequently, at z = 12 cm the vertical velocity spectrum flattens at about k_1 = 60 rad/m, i.e., $l \approx$ 10 cm, and at z = 44 cm the flattening starts at a k_1=15, corresponding to $l \approx$ 40 cm.

At small scales E_{11} and E_{33} converge to similar slopes. In all cases the range of wavenumbers where a (-5/3) slope line can be fitted does not exceed a decade. At the lowest station (z = 12 cm), this range is even smaller. For isotropic turbulence, in the inertial range, $E_{11}(k_1) = 3/4\ E_{33}(k_1)$, a condition that is clearly not satisfied in the present data.

Sample "dissipation spectra" (Tennekes and Lumley, 1972), i.e. plots of $k_1^2 E_{ii}$, are presented in Figure 3, in both linear and logarithmic scales. The plots of the streamwise fluctuations ($k_1^2 E_{11}$) do not tail off at high wavenumbers due to noise. The plots of $k_1^2 E_{33}$ exhibit clear peaks at $k_1 \approx$ 100-150 rad/m suggesting that the wavelength of peak dissipation is 4-6 cm. Thus, the present data extends to wavenumbers in the dissipation range.

We evaluated several methods to estimate the dissipation rate, ε, of which three are only possible with 2-D spatial distributions of velocity. The first method is based on the exact definition of dissipation rate $\varepsilon = -2\nu S_{ij} S_{ij} = \nu\, \partial u_i / \partial x_j \left(\partial u_i / \partial x_j + \partial u_j / \partial x_i \right)$. Using planar PIV we can measure five of these terms directly, and the sixth can be determined from the

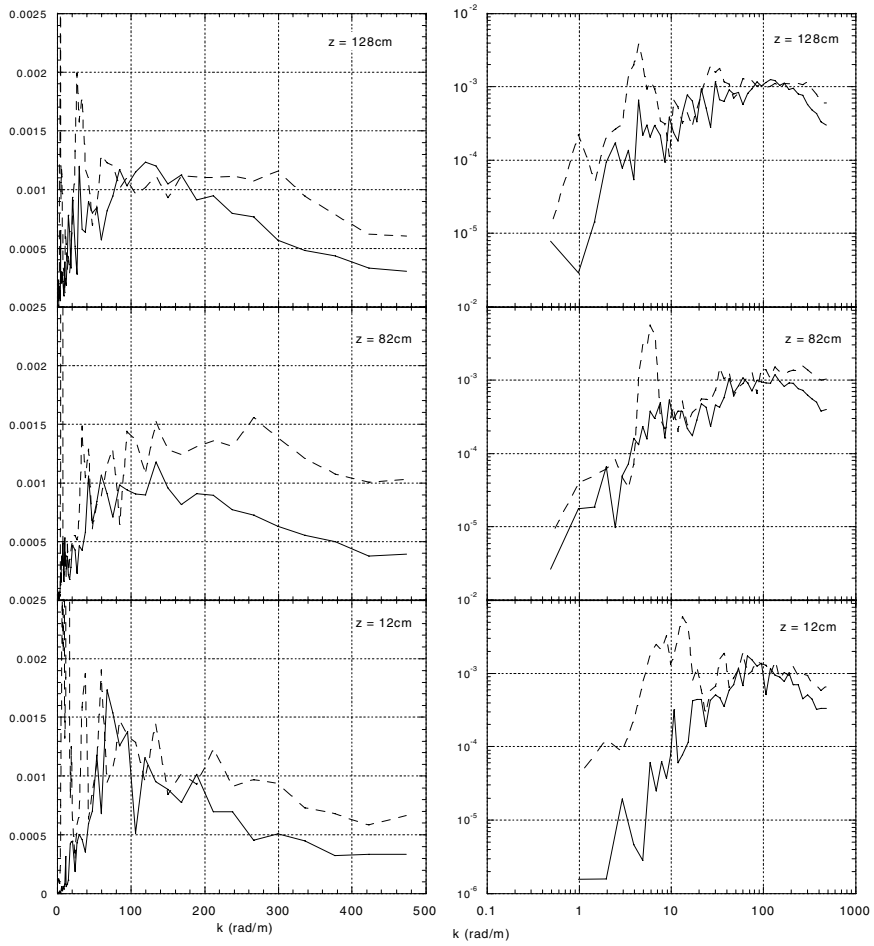

Figure 3: Sample dissipation spectra calculated from the extended vector maps. Solid lines: $k_1^2E_{33}$; dashed lines: $k_1^2E_{11}$ Sample below: a fitted Nasmyth curve to a sample spectrum (shown in linear scales).

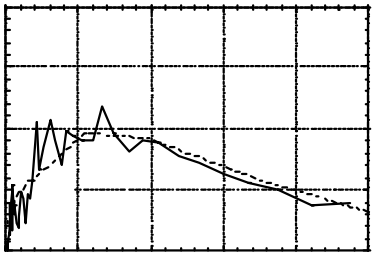

continuity equation. For isotropic turbulence the known terms represent 8/15 of the total dissipation. Additional terms are estimated, assuming that all lateral fluctuations have similar average magnitudes, leading to a "direct estimate of dissipation:

$$\varepsilon_D = 3\nu\left[\left\langle\left(\frac{\partial u}{\partial x}\right)^2\right\rangle + \left\langle\left(\frac{\partial w}{\partial z}\right)^2\right\rangle + \left\langle\left(\frac{\partial u}{\partial z}\right)^2\right\rangle + \left\langle\left(\frac{\partial w}{\partial x}\right)^2\right\rangle + 2\left\langle\left(\frac{\partial u}{\partial z}\frac{\partial w}{\partial x}\right)\right\rangle + \frac{2}{3}\left\langle\left(\frac{\partial u}{\partial x}\frac{\partial w}{\partial z}\right)\right\rangle\right]$$

The only assumption is that cross-stream gradients are have the same average magnitude as the measured in-plane cross gradients. In isotropic turbulence these assumptions become identities. The second method is based on the hypothesis that the turbulence is locally axisymmetric (e.g., George and Hussein, 1991, Antonia et al., 1991). This assumption is less stringent than the requirements for isotropy and leads to:

$$\varepsilon_{AS} = \nu\left[-\left(\frac{\partial u}{\partial x}\right)^2 + 8\left(\frac{\partial w}{\partial z}\right)^2 + 2\left(\frac{\partial u}{\partial z}\right)^2 + 2\left(\frac{\partial w}{\partial x}\right)^2\right]$$

The third method involves an assumption of isotropic, homogeneous turbulence, at least in the inertial range, which is not accurate for the present data. As shown in Hinze (1975) and Tennekes and Lumley (1972), $E_{11}(k_1) = 18/55\,(1.6)\varepsilon_{LF}^{2/3}k_1^{-5/3}$:

Since the streamwise velocity spectra are more susceptible to contamination by surface waves, we evaluate the dissipation rate, ε_{LF}, from the spectra of the vertical component, based on the isotropic ratio of $E_{11}=4/3E_{33}$. The estimates of ε_{LF} are obtained by fitting the Nasmyth universal spectrum (Oakey, 1982) in the inertial range only. This method is similar to that proposed by Stewart and Grant (1962). The fourth estimate is based on integrating the dissipation spectrum (Monin and Yaglom, 1975):

$$\varepsilon_{DS} = \frac{15}{2}\nu \int_0^\infty k_1^2 E_{33}(k_1) dk_1$$

Since the present data does not extend to the Kolmogorov scale and the results in Figure 3 show effects of noise , we fit a Nasmyth universal spectrum to our data (matching values in the noise-free region, see Doron et al., 1999 for details) and then integrate the universal spectrum. Finally, in Large Eddy Simulation (LES) of turbulent flows we introduce a Sub Grid Stress (SGS) Tensor $\tau_{ij} = \widetilde{u_i u_j} - \tilde{u}_i \tilde{u}_j$ where "~" indicates spatial filtering. If the scale of the filtering is performed in the inertial range, the condition of equilibrium suggests that the energy flux to smaller (subgrid) scales should provide an estimate of the dissipation rate (Liu et al., 1994, 1999). Thus, $\varepsilon_{SG} = -\tau_{ij}\tilde{S}_{ij}$, where S_{ij} is the filtered rate of strain. Using assumptions of equality of cross components we obtain

$$\varepsilon_{SG} = \frac{1}{2}\left(3\tau_{11}\tilde{S}_{11} + 3\tau_{33}\tilde{S}_{33} + 12\tau_{13}\tilde{S}_{13}\right)$$

As shown in Table 1, the various methods provide comparable but different results (the curve-fitted results are higher). Thus, even in the present anisotropic turbulence, estimates of dissipation based on isotropy lead to reasonable results.

TABLE I

Elevation (cm)	"Direct"		ε_{LF} x 10^6 (m^2/s^3)	ε_{DS} x 10^6 (m^2/s^3)	ε_{AS} x 10^6	ε_{SG} x 10^6 (m^2/s^3)
	ε_D x 10^6	η (mm)				
128	3.9	0.92	5.8	4.3	3.7	4.8
106	6.0	0.82	8.8	8.2	5.3	10.5
82	3.3	0.95	5.2	4.1	3.0	3.6
62	4.1	0.90	7.3	5.7	3.7	5.8
44	3.1	0.97	3.7	3.2	2.8	2.8
12	4.1	0.90	4.5	4.1	3.9	7.9

Long data Series: With the long data series we obtain considerably smoother velocity distributions as demonstrated by the sample shown in Figure 4. Tests also show that the turbulence parameters are fully converged when the data base exceeds 1000 vector maps (we have > 1800). The sample shown extends between 10-30 cm above the bottom. A least-square fit to a logarithmic curve is also presented. Note that although there seems to be a close match, the results clearly deviate from a log curve (the line is not straight in the semi-log plot). Besides converged statistics, the extended data series also provides spectra that extend over four orders of magnitude of scales.

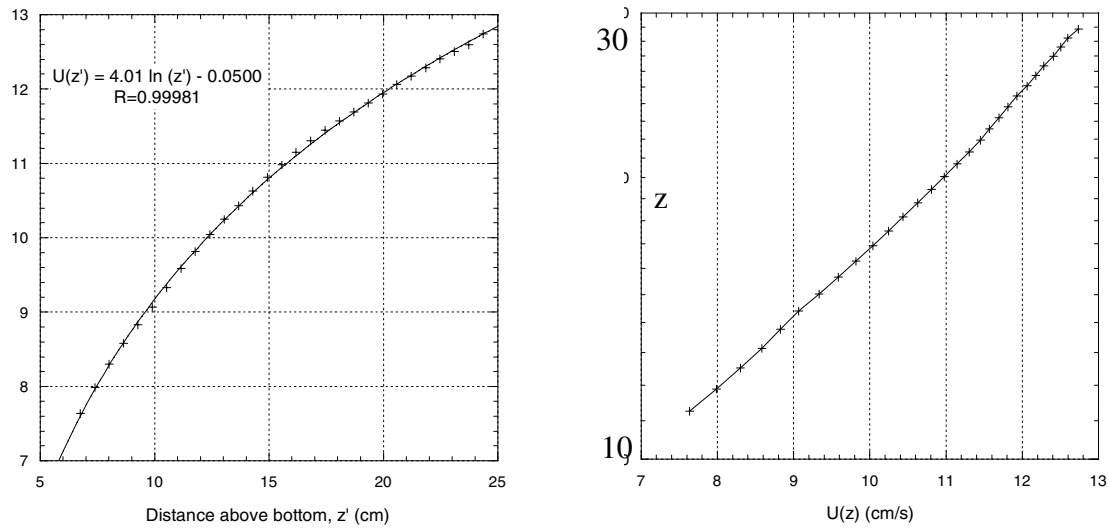

Figure 4: A logarithmic curve fit to the long data series. The same result is shown on linear and semi-log scales to illustrate trends.

IMPACT/APPLICATIONS

The present measurements allow us to test fundamental assumptions about turbulence in the oceanic bottom boundary layer; specifically the existence of logarithmic profile, the applicability of Taylor's hypothesis, methods to estimate dissipation and the dissipation-production balance. In the future we intend to look at flow structures, vorticity transport and evaluate turbulence models. Since the images contain information about the particle distributions, we will also relate the sediment transport and turbulence.

TRANSITIONS

During FY 2000 the submersible PIV system will be used at NSWC/Carderock to measure the flow structure within wakes behind maneuvering submerged models.

REFERENCES

Antonia, R.A., J. Kim, and L.W.B. Browne, 1991: Some characteristics of small-scale turbulence in a turbulent duct flow. *J. Fluid Mech.*, 233: 369–388.

George, W.K., and H.J. Hussein, 1991: Locally axisymmetric turbulence. *J. Fluid Mech.*, 233: 1–23.

Hinze, J.O., 1975: *Turbulence*. 2nd ed. McGraw-Hill, New York, New York.

Liu, S., C. Meneveau, and J. Katz, 1994: On the properties of similarity subgrid-scale models as deduced from measurements in a turbulent jet. *J. Fluid Mech.*, 275: 83–119.

Monin, A.S., and A.M. Yaglom, 1975: *Statistical Fluid Mechanics: Mechanics of Turbulence*. Vol. 2, MIT Press, Cambridge, Massachusetts.

Oakey, N.S., 1982: Determination of the rate of dissipation of turbulent energy from simultaneous temperature and velocity shear microstructure measurements, *J. Phys. Oceanogr.*, 12: 256–271.

Stewart, R.W., and H.L. Grant, 1962: Determination of the rate of dissipation of turbulent energy near the sea surface in the presence of waves. *J. Geophys. Res.*, 67(8): 3177–3180.

PUBLICATIONS

Bertuccioli, L., Roth, G.I., Katz, J., Osborn, T.R., (1999), "Turbulence Measurements In The Bottom Boundary Layer Using Particle Image Velocimetry", Journal of Atmospheric and Oceanographic Technology, Vol. 16, No. 11, Part 1, pp. 1635-1646.

Doron, P., Bertuccioli, L., Katz, J., Osborn, T.R., (1999), "Turbulence Characteristics and Dissipation Estimates in The Coastal Ocean Bottom boundary Layer from PIV Data," submitted for publication in Journal of Physical Oceanography.

Doron, P., Bertuccioli, L., Katz, J., Osborn, T.R., (1999), Particle Image Velocimetry Measurements of Turbulence Over The Coastal Ocean Floor," Proceedings of FEDSM'99, 3rd ASME/Joint Fluids Engineering Conference, July 18-23, San Francisco, CA, paper No. FEDSM99-7263.

Bertuccioli, L., Doron, P., Katz, J., Osborn, T., (1998), "Particle Image Velocimetry (PIV) measurements Of turbulence Near The Ocean Floor," American Geophysical Union Meeting, Fall 1998, Abs. No. 15462.